iScience

CellPress
OPEN ACCESS

Article

# Hydroxyapatite catalyzed hydrothermal liquefaction transforms food waste from an environmental liability to renewable fuel

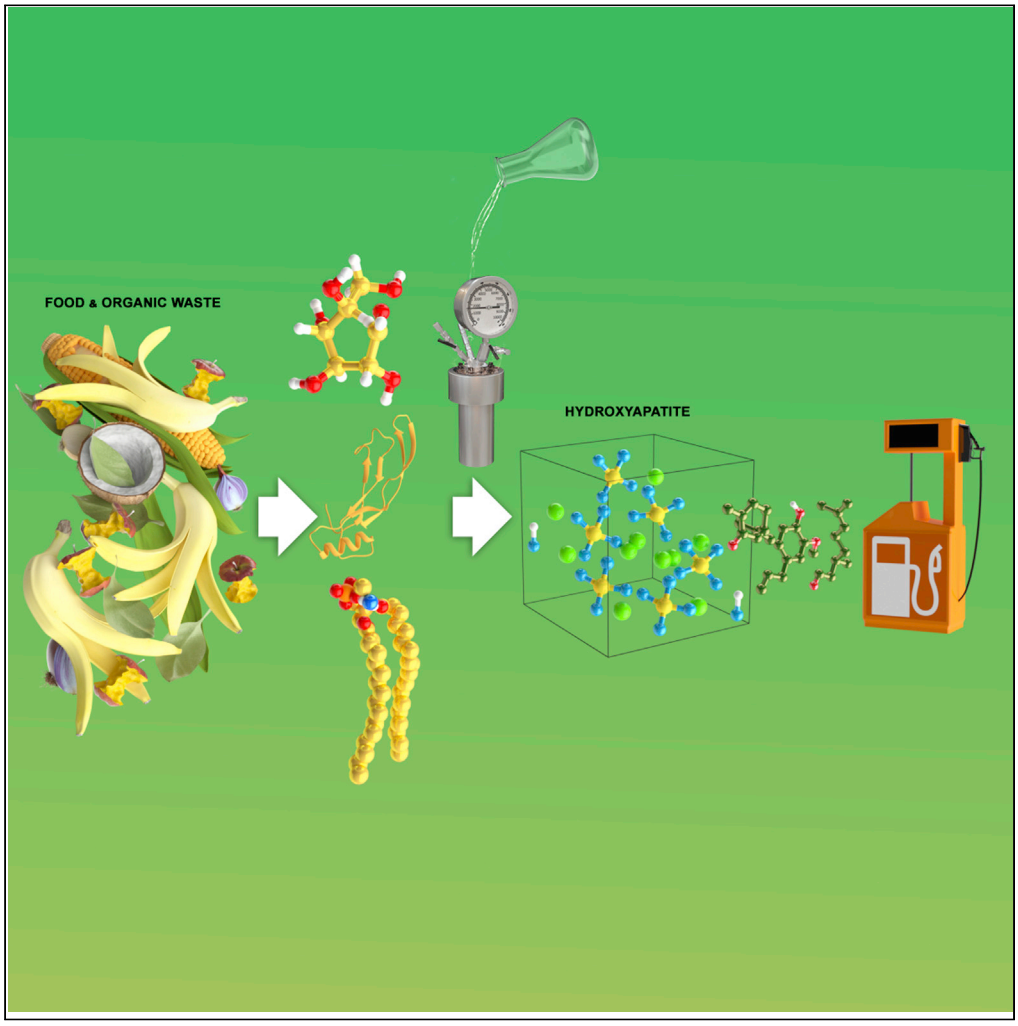


Heather O. LeClerc, Geoffrey A. Tompsett, Alex D. Paulsen, ..., Feng Cheng, Andrew R. Teixeira, Michael T. Timko

mttimko@wpi.edu

## Highlights

Catalysts boost yields obtained from hydrothermal liquefaction (HTL) of food waste

HAP-catalyzed HTL has the potential to reduce US greenhouse gas emissions by 2.6

Catalytic food waste HTL can produce fuel with an MFSP of $1.06/GGE

LeClerc et al., iScience 25, 104916
September 16, 2022 
https://doi.org/10.1016/j.isci.2022.104916

iScience

CellPress
OPEN ACCESS

Article

# Hydroxyapatite catalyzed hydrothermal liquefaction transforms food waste from an environmental liability to renewable fuel

Heather O. LeClerc,[1] Geoffrey A. Tompsett,[1] Alex D. Paulsen,[2] Amy M. McKenna,[3,4] Sydney F. Niles,[3] Christopher M. Reddy,[5] Robert K. Nelson,[5] Feng Cheng,[1] Andrew R. Teixeira,[1] and Michael T. Timko[1,6,*]

## SUMMARY

**Food waste is an abundant and inexpensive resource for the production of renewable fuels. Biocrude yields obtained from hydrothermal liquefaction (HTL) of food waste can be boosted using hydroxyapatite (HAP) as an inexpensive and abundant catalyst. Combining HAP with an inexpensive homogeneous base increased biocrude yield from 14 ± 1 to 37 ± 3%, resulting in the recovery of 49 ± 2% of the energy contained in the food waste feed. Detailed product analysis revealed the importance of fatty-acid oligomerization during biocrude formation, highlighting the role of acid-base catalysts in promoting condensation reactions. Economic and environmental analysis found that the new technology has the potential to reduce US greenhouse gas emissions by 2.6% while producing renewable diesel with a minimum fuel selling price of $1.06/GGE. HAP can play a role in transforming food waste from a liability to a renewable fuel.**

## INTRODUCTION

Over 1.3 billion tons of food is wasted worldwide every year (Schanes et al., 2018). In the United States, over 63 million tons of food is discarded annually, including manufacturing, residential, and commercial waste (Agency, 2021b). Food waste is energy dense and has the potential for production of fuels and chemicals (Pfaltzgraff et al., 2013). Multi-step conversion to usable energy has shown promise as a more sustainable approach to food waste management than current practices (Paritosh et al., 2017). Unfortunately, most food waste is discarded in landfills with non-substantive energy recovery occurring with 6.3% of the disposal going toward incineration with energy recovery (EPA, 2020). However, if 100% of the world's annual supply of wasted food was converted to usable energy, it could power the United States for two years based on the 2020 energy consumption rate (Administration, 2021b; Ouadi et al., 2019).

Hydrothermal processes have recently gained attention for the conversion of biomass, algal, and organic wets wastes into fuels, chemicals, and materials (Castello et al., 2018; Gollakota et al., 2018). Unlike dry thermal conversion technologies (e.g., pyrolysis and gasification), hydrothermal processes are compatible with wet feeds (Castello et al., 2018; Gollakota et al., 2018). Compared with anaerobic digestion (days), hydrothermal processes are rapid (minutes), making them appropriate for modular, distributed deployment (Bielenberg and Palou-Rivera, 2019).

HTL has been extensively studied for use with algal and sludge feedstocks (Gollakota and Savage, 2020; Du et al., 2013; Gollakota et al., 2018; Peterson et al., 2008), primarily to maximize biocrude yield. Maximizing the lipid content of algae benefits HTL biocrude yields. However, the National Renewable Energy Laboratory (NREL) has estimated the minimum algae feedstock costs to be $430/ton ash free dry weight (AFDW) (Ryan Davis et al., 2016), and experimental values are above $1,000/ton (Jiang et al., 2019), which makes conversion of algae into liquid fuels economically infeasible.

Utilizing food waste as a feedstock for HTL can replace the high cost of algae cultivation with feedstocks that have negative costs (Kantner, 2019). Unfortunately, biocrude yields obtained from HTL processing of food waste are much less than those obtained from algae, a feed that is rich in biocrude forming lipids (Cheng et al., 2017, 2020; Maag et al., 2018). Of importance, additional research is needed to make efficient

[1]Department of Chemical Engineering, Worcester Polytechnic Institute, 100 Institute Road, Worcester, MA 01609, USA

[2]Mainstream Engineering Corporation, 200 Yellow Place, Rockledge, FL 32955, USA

[3]National High Magnetic Field Laboratory, 1800 Paul Dirac Dr., Tallahassee, FL 32310, USA

[4]Department of Soil & Crop Sciences, Colorado State University, Fort Collins, CO 80523, USA

[5]Woods Hole Oceanographic Institution, 86 Water St., Falmouth, MA 02543, USA

[6]Lead contact

*Correspondence: mttimko@wpi.edu

https://doi.org/10.1016/j.isci.2022.104916

use of abundant, inexpensive organic wet waste streams, (e.g., food waste) while matching biocrude yields that can be obtained from expensive high-lipid algae.

One approach to improving biocrude yields obtained from HTL processing of low-cost feeds is to use a catalyst (Nagappan et al., 2021). Although catalytic HTL has been reported previously in the literature, its impact has been limited by catalyst costs, especially when considering the harsh conditions that prevail during HTL (Azadi and Farnood, 2011; Besson et al., 2014; Cheng et al., 2021). Inexpensive, abundant, stable, and effective catalysts are required to make catalytic HTL of wet waste streams economically competitive (Maag et al., 2018).

Hydroxyapatite (HAP), a naturally occurring mineral consisting of calcium and phosphorous oxides found in bone with the molecular formula $Ca_{10}(PO_4)_6(OH)_2$, meets all of these criteria (Fihri et al., 2017). HAP is thermally stable in air at temperatures <700°C (Roberts et al., 2015; Mostafa, 2005). The hydrothermal stability of HAP has not been examined in detail; however, Roberts et al. reported the formation of HAP from calcium and phosphorous precursors naturally present in microalgae during HTL, implying that HAP is stable at HTL conditions (Roberts et al., 2015). The acid and base properties of HAP can be tuned by altering the pH between 7 and 11 during synthesis to manipulate the coordination of oxygen around the central calcium atom and result in a range of base to acid site ratios (Fihri et al., 2017; Tsuchida et al., 2006). HAP's use in biomass conversion and for promoting HTL reactions is relatively unexplored; however, others have catalyzed carbon-carbon cross-coupling, condensation, and oxidation reactions (Kaneda et al., 2004; Tsuchida et al., 2008b; Fihri et al., 2017; Kiani and Baltrusaitis, 2021). Understanding these pathways at the molecular level therefore is a further requirement for HTL to be impactful (Cheng et al., 2021).

The objective of this work was to evaluate the use of HAP for improving biocrude yields obtained from HTL of organic wet waste and to characterize biocrude compositions as a basis for chemically resolved biocrude formation models. HTL product distributions, including biocrude yields, were measured for HTL of a model food waste stream using a series of HAP materials with varying acid-base properties. The recovered catalyst was studied after initial use, after prolonged exposure to hydrothermal conditions, and as part of a new method for converting carbon lost to the HTL aqueous phase into biocrude to further understand the role of the catalyst in condensation reactions. Biocrude and aqueous phase products were analyzed using molecular level methods to develop a basis for chemically resolved biocrude formation models that can guide process development. Lastly, experimental data were input into economic and environmental models to predict potential outcomes. The results and analysis presented here establish a new technological and scientific baseline for the use of catalytic HTL as a method to transform environmental liabilities into renewable fuels.

## RESULTS AND DISCUSSION

### Catalyst characterization and performance evaluation

Each of the six HAP catalysts was tested to establish effectiveness at promoting biocrude formation in the hydrothermal conversion of a model food-waste mixture. The HAP catalysts were selected to represent a range of calcium-to-phosphorus ratios, because this property correlates with catalytic performance in many important reactions (Tsuchida et al., 2008a). Accordingly, catalysts are named "HAP" for hydroxyapatite with a suffix that denotes the calcium-to-phosphorous ratio of the material. Experiments were performed in the absence of catalyst as a control.

Figure 1 provides the product yields observed for these experiments, reported in terms of mass yield as a percent of the organic loading. Mass balance closure was always greater than 90% and error – ascertained by comparison of multiple runs – was less than 8%.

Addition of HAP increased biocrude mass yield (Figure 1) from a value of 13.6% in the absence of catalyst to 40.7% for HAP-1.86. The average biocrude yield in the presence of HAP was 29.7%, indicating the importance of specific HAP properties. Biocrude yield was weakly dependent on calcium-to-phosphorus ratio, with the three materials with Ca/p > 1.5 resulting in greater biocrude yields than the three materials with Ca/p < 1.5. Figure S1 re-plots product fractions on a carbon basis, wherein HAP-1.86 shows increased oil-phase carbon compared to the thermal case.

Table 1 provides additional detail on the various biocrudes obtained using HAP and in the control run. Biocrude elemental composition is within the range 60–70 wt% carbon, 8–9 wt% hydrogen, 17–27 wt% oxygen, and 3–4 wt% nitrogen. The higher heating values (HHVs) of the biocrude samples were measured

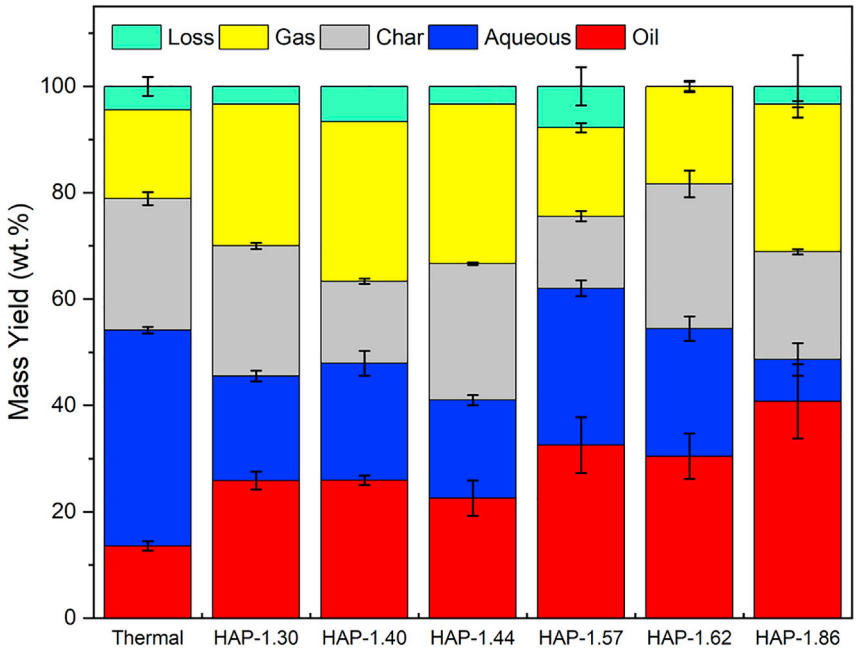


**Figure 1. HAP-catalyzed hydrothermal liquefaction product yields**

Product yields for all phases of HAP catalyzed hydrothermal liquefaction. Product yields reported in mass percent of organic feed. Oil is equivalent to biocrude. All reactions utilized 5% wt % catalyst completed at 300°C, 1 h residence time, and 15% solids loading. See also Figure S1 and Table S2.

independently from composition and found to vary from 31 to 38MJkg$^{-1}$ (measurement uncertainty = ±1MJkg$^{-1}$). The biocrude obtained from use of HAP-1.86 contains the most carbon, only slightly higher than that from thermal HTL, yet its energy recovery is 3.5 times greater. This finding indicates the need for further analytical characterization for more accurate analysis compared to the bulk.

Table 1 shows that the energy recovery obtained using HAP-1.86 was substantially (~25%) greater than any other catalyst. Accordingly, HAP-1.86 was evaluated in more detail and its superior performance was found to arise from the presence of labile base sites on its surface as indicated by surface titration before and after rinsing (Tables S1 andS2). Figure S2 provides biocrude yields obtained from tests on a rinsed version of HAP-1.86 and the corresponding supernatant liquid, showing that both of these increased biocrude yield relative to that observed under non-catalytic conditions. The energy recovery observed for HAP-1.86 after rinsing is comparable within the limits of uncertainty to those observed for HAP-1.57 and HAP-1.62. Of interest, the individual improvements of the supernatant and the washed HAP appear to be additive, causing the same improvement observed using HAP-1.86 in its original state (within the limits of experimental uncertainty). Subsequent experiments with rinsed HAP-1.86 and homogeneous base (Figure S2) show that the combination of heterogeneous and homogeneous catalysts greatly increases biocrude yields obtained by HTL relative to either one used on its own.

The various HAP-based catalysts were characterized in greater detail for textural, composition, and surface properties. Figures S3, S4, S5, S6, S7 S8 andS9 contain XRD, SEM, and nitrogen sorption curves. Catalyst properties were studied after use and after 200-h endurance tests in liquid water at 300°C. In summary, the key characteristics required for boosting energy recovery are surface area greater than 20 $m^2g^{-1}$, balanced presentation of acid and base sites (Tsuchida et al., 2006, 2008a), stability after use and after long-term liquid water exposure (200 h), and most importantly, a calcium-to-phosphorous ratio greater than 1.50.

One problem revealed by catalyst characterization after use was accumulation of char on the surface that will lead to its de-activation over time (Stummann et al., 2019), a consequence of direct contact between the biopolymers contained in the feed with the catalyst during what can be termed *in situ* catalytic HTL. Removing the catalyst from the HTL reactor and instead using it in a secondary reactor to recover oil that would otherwise be lost to the aqueous phase has the potential to limit char accumulation by removing

**Table 1. HTL biocrude properties from thermal and catalytic hydrothermal liquefaction at 300°C and 200 bar**

| Conditions | C (wt %) | H (wt %) | N (wt %) | O (wt %)[a] | Oil Yield (%) | HHV (MJ/kg) | Energy Recovery (%) |
|---|---|---|---|---|---|---|---|
| Food Waste | 47.2 | 6.7 | 4.6 | 41.5 | N/A | 24.6 | N/A |
| Thermal | 69.9 | 8.4 | 3.8 | 17.9 | 14 ± 1 | 32.1 | 18 ± 2 |
| HAP-1.30 | 68.1 | 8.5 | 2.8 | 20.6 | 26 ± 3 | 33.5 | 35 ± 3 |
| HAP-1.40 | 60.3 | 8.4 | 3.5 | 27.8 | 26 ± 5 | 32.2 | 34 ± 5 |
| HAP-1.44 | 67.3 | 8.8 | 2.9 | 21.0 | 23 ± 7 | 33.5 | 31 ± 7 |
| HAP-1.57 | 68.0 | 9.2 | 3.1 | 19.1 | 33 ± 5 | 35.4 | 47 ± 4 |
| HAP-1.62 | 67.7 | 8.3 | 3.2 | 20.8 | 31 ± 4 | 31.0 | 38 ± 4 |
| HAP-1.86 | 70.3 | 9.0 | 3.7 | 17.0 | 41 ± 5 | 38.3 | 63 ± 5 |

Elemental analysis (CHNO) percentages for the biocrude phase, oil yield, higher heating value, and energy recovery of all HAP and thermal runs.
[a]Oxygen weight by difference.

it from direct contact with biopolymer present in the feed (Lucian et al., 2018). Following terminology usage in pyrolysis (Wan and Wang, 2014), using the catalyst in a separate reactor than used for HTL can be termed *ex situ* catalytic HTL.

The biocrude yields obtained from *in situ* and *ex situ* catalytic HTL experiments are shown in Figure 2, using HAP-1.86 as a model catalyst. Figure 2 indicates that nearly 36% of the carbon remaining in the aqueous phase can be converted to biocrude by use of *ex situ* catalysis. Summing the biocrude obtained from thermal processing and *ex situ* carbon recovery corresponded to a biocrude carbon yield of 49%, which is the same as that obtained under *in situ* conditions using the same catalyst within estimated limits of experimental uncertainty. Unlike for *in situ* catalyst use, which accumulated 5–15 wt% carbon on the surface as char, the carbon content of the catalyst used under *ex situ* conditions was less than 1 wt%. Figure S10 contains photographs of the various catalysts. These results indicate that *ex situ* use of the HTL catalyst retains all of the benefits of using a catalyst without the problems associated with carbon accumulation on the surface.

## Molecular level analysis

Table 1 presents bulk properties of the HTL biocrudes. However, it lacks the molecular level detail required for science-based reactor design and upgrading. The next step was molecular characterization of the biocrude product to understand its formation pathways to guide rational design of the HTL process.

Biocrude formation consists of a complicated sequence of biopolymer depolymerization and rearrangement into oil-soluble products. The lipid content of food waste is insufficient to explain the biocrude yields obtained here (Table 1). In addition to lipids, food waste contains starch, proteins, and simple carbohydrates that must contribute to biocrude formation to explain the observed yields. Understanding how the presence of a catalyst promotes participation of the carbohydrates and proteins in biocrude formation is therefore key to utilization of low-lipid feeds for HTL. Reaction pathways of particular interest therefore are ones that convert water-soluble molecules, such as simple carbohydrates and amino acids, into oil-soluble ones that contribute to biocrude formation.

As a complex, multi-component mixture, partitioning of a single molecule into biocrude is not well defined. The octanol-water partition coefficient ($K_{ow}$) offers a convenient and quantitative proxy to understand biocrude-water partitioning (Kumar et al., 2015). Unlike biocrude-water partition coefficients, octanol-water partition coefficients have been measured for many compounds of interest (Sangster, 1989), and empirical methods are available for predicting octanol-water partition coefficients for compounds that have not been studied previously (Meylan et al., 1996; Zissimos et al., 2002). Moreover, octanol-water partition coefficients have proven to be linearly related to partition coefficients of many poorly defined thermodynamic systems (Hu et al., 2018; Budhwani, 2015), recommending their use for quantitative description of biocrude partitioning. Accordingly, $K_{ow}$ is used here to guide the understanding of what compounds should contribute to biocrude formation.

The various HTL products were analyzed at the molecular level using GC×GC, FT-ICR MS, and FT-IR spectroscopy. Each instrument served a specific purpose, with GC×GC analysis used to obtain precise molecular

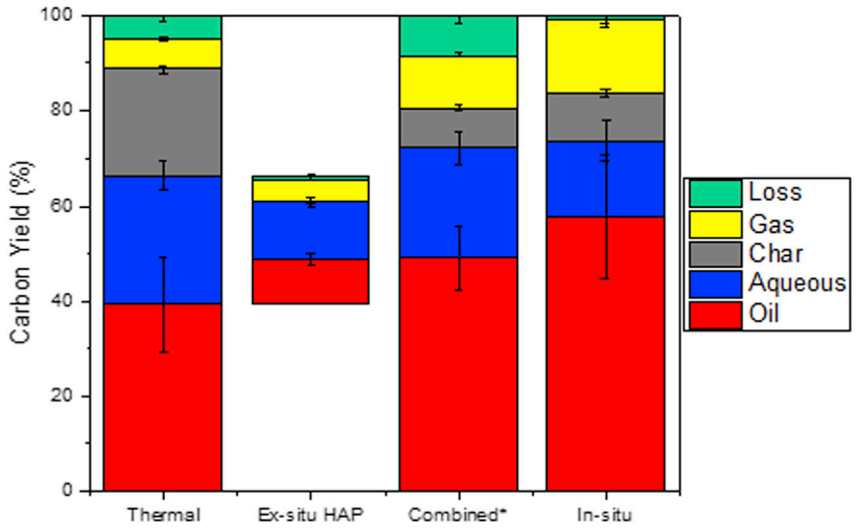


**Figure 2. HAP-catalyzed *ex situ* carbon yields**

Ex-situ carbon yields for oil, aqueous, solid, and gas phases. *Ex-situ* experiments utilized thermal aqueous phase as the HTL feedstock with 5 wt% HAP-1.86 catalyst. The bar corresponding to *ex situ* HAP is sized equally to the thermal aqueous phase to show the percentage of aqueous feed converted to biocrude. *Denotes mathematical combination of thermal and *ex situ* runs. All runs depict the average thermal yield without catalyst addition. Conditions: 300°C, 1 h, 200 bar. See also Table S1 and Figure S2.

structure information for volatile products; (+) APPI FT-ICR MS was used to obtain isotopically accurate elemental formulas of ionizable species with molecular weights >150 Da; and FT-IR spectroscopy used to identify functional groups regardless of molecular weight. Data from these methods – especially GC×GC and FT-ICR MS – were then used to reconstruct biocrude and aqueous phase composition and thereby develop a framework for biocrude formation.

Figure 3 contains GC×GC-FID chromatograms corresponding to the biocrude obtained under non-catalytic conditions. Figure S11 contains chromatograms with identical first and second dimension retention times obtained from analysis of biocrudes obtained in the presence of *in situ* catalysts. Qualitatively, the chromatograms obtained in the presence and absence of a catalyst are similar to one another. Two-dimensional GC analysis shown in Figure 3A leads to multiple groupings of chemical classes, identifying $C_8$ – $C_{20}$ fatty acids as the major biocrude products. Fatty acids arise from hydrolysis of triglycerides and possess $K_{ow} \gg 10$, consistent with partitioning into the biocrude phase (Simpson et al., 1974).

Secondarily, Figure 3A indicates the presence of n-alkenes, the products of fatty acid decarboxylation, and fatty amides, represented by a cluster of peaks that elute at retention times greater than the corresponding fatty acids. Fatty amides are the putative products formed by reaction of fatty acids with amino acids and especially their breakdown products, including amines (90%) and methyl amines (10%) (Betancourt-Jimenez et al., 2020; Cheng et al., 2017). As with the fatty acids, the $\log(K_{ow})$ of fatty amides with more than ten carbon atoms is predicted to be greater than 10. Moreover, the abundance of fatty amides establishes the importance of C-N formation reactions as a biocrude formation pathway, because the amino acid reactants on their own are predicted to partition into the aqueous phase ($\log(K_{ow}) < 2$).

Aside from the abundant fatty acids and amides, Figure 3A indicates the presence of numerous trace-level peaks eluting earlier in the first dimension than the fatty acids. As identified by their corresponding mass spectra, these compounds belong to several classes, including cresols and indoles, highlighted in Figure 3. Figure 3C shows a zoomed in portion of the GC×GC chromatogram showing a series of alkyl phenols (cresols), with between one and four carbons present as side chains, shown in Figure 3B. The cresols and indoles form from reactions of carbohydrates with one another (Sad et al., 2008) or with amino acids (Lamping et al., 2015; Meshram et al., 2013). Unlike the parent compounds, which are expected to be water soluble, these molecules possess $\log(K_{ow})$ values >10, consistent with biocrude forming molecules. Detailed mass spectra are provided in the Supporting Information as Figure S12 and FT-IR in Figure S13.

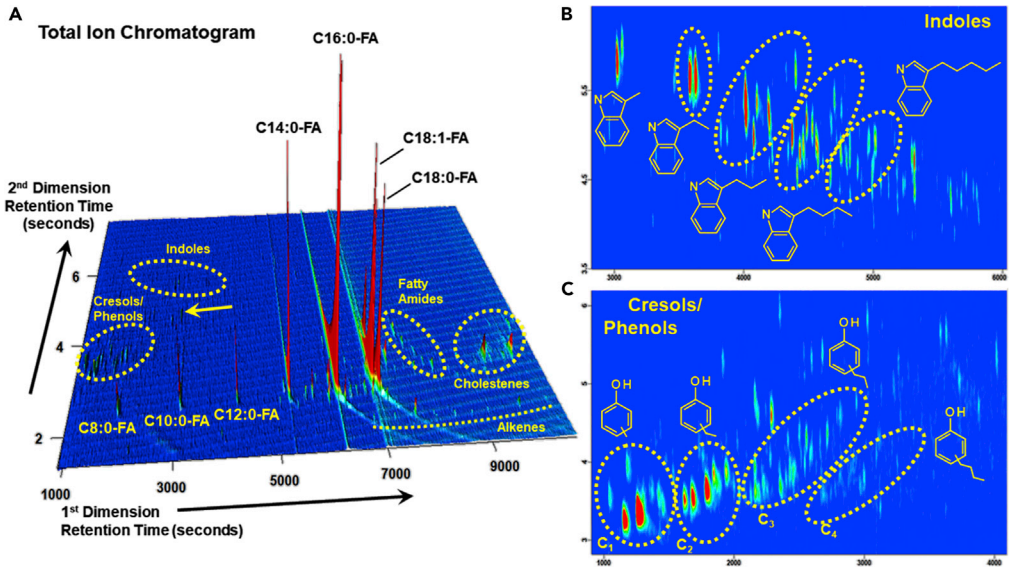


**Figure 3. Two-dimensional gas chromatography highlights primary biocrude product classes**

(A) GC×GC-FID total ion mountain plot chromatograms of biocrude obtained from non-catalytic food waste HTL.

(B) GC×GC chromatogram depicting the area showing a range of substituted indoles.

(C) GC×GC chromatogram depicting the range of substituted phenols and cresols. See also Figures S11 and S12.

Despite GC analysis providing molecularly detailed information, thermal analysis indicates that less than 45% of the biocrude is volatile enough for GC analysis. Accordingly, (+) APPI FT-ICR MS was used to determine isotopically accurate molecular formulas of the ionizable heavy fraction of the biocrude (>150 Da). (+) APPI FT-ICR MS is especially sensitive to aromatic compounds and is capable of ionizing molecules across a broad range of polarities, especially relevant because of biocrude complexity (Purcell et al., 2007a; Robb and Blades, 2006; He et al., 2021).

Figure 4contains double-bond equivalency (DBE) data as a function of the number of carbon atoms for the six most abundant heteroatom classes identified in Figure S14. As more nitrogen and oxygen are incorporated into the molecule, the average carbon number and DBE also increases, as required to maintain $K_{ow}$ values that favor biocrude formation.

In theory, a vast number of molecules can give rise to the FT-ICR MS patterns shown in Figure 4. In practice, the molecular structures indicated by FT-ICR MS must be consistent both with the components known to be present in the volatile biocrude fraction and known chemical pathways. The consistency requirement makes tractable the assignment of probable molecular classes to the FT-ICR MS data. The results are provided as part of Figure 4, which shows that combinations of indoles and fatty acids, compounds that can be termed fatty indoles, are predicted to be especially prevalent in the biocrude. Of interest, to remain consistent with the predicted DBE and GC×GC, fatty acids are proposed to form bonds with the indole both through the nitrogen atom, the result of an amidation reaction, and through formation of C-C bonds, indicating multiple probable mechanisms for fatty indole formation. Similarly, Figure 4 provides $K_{ow}$ values for representative molecules of these different classes, showing that these products are predicted to partition into the biocrude phase. Analysis of the biocrude formed by *ex situ* catalysis points toward a process involving coupling of water-soluble products into oil soluble ones, thereby resulting in carbon transfer from the aqueous phase to the biocrude. Of interest, *ex situ* catalysis seems to especially favor amidation reactions, as indicated by the C-N stretch that is much more intense in the *ex situ* biocrude sample compared with the others and as shown in Figure S13 (Lu et al., 2018).

Figure 5 extends this analysis to explore the relationship of molecular weight and heteroatom class, containing a plot of abundance of different heteroatom classes as functions of molecular weight. The number of heteroatoms present in the biocrude molecules generally decreases with decreasing molecular weight, thereby maintaining favorable $K_{ow}$ values across the entire molecular weight spectrum. More information is provided in Figure S15,

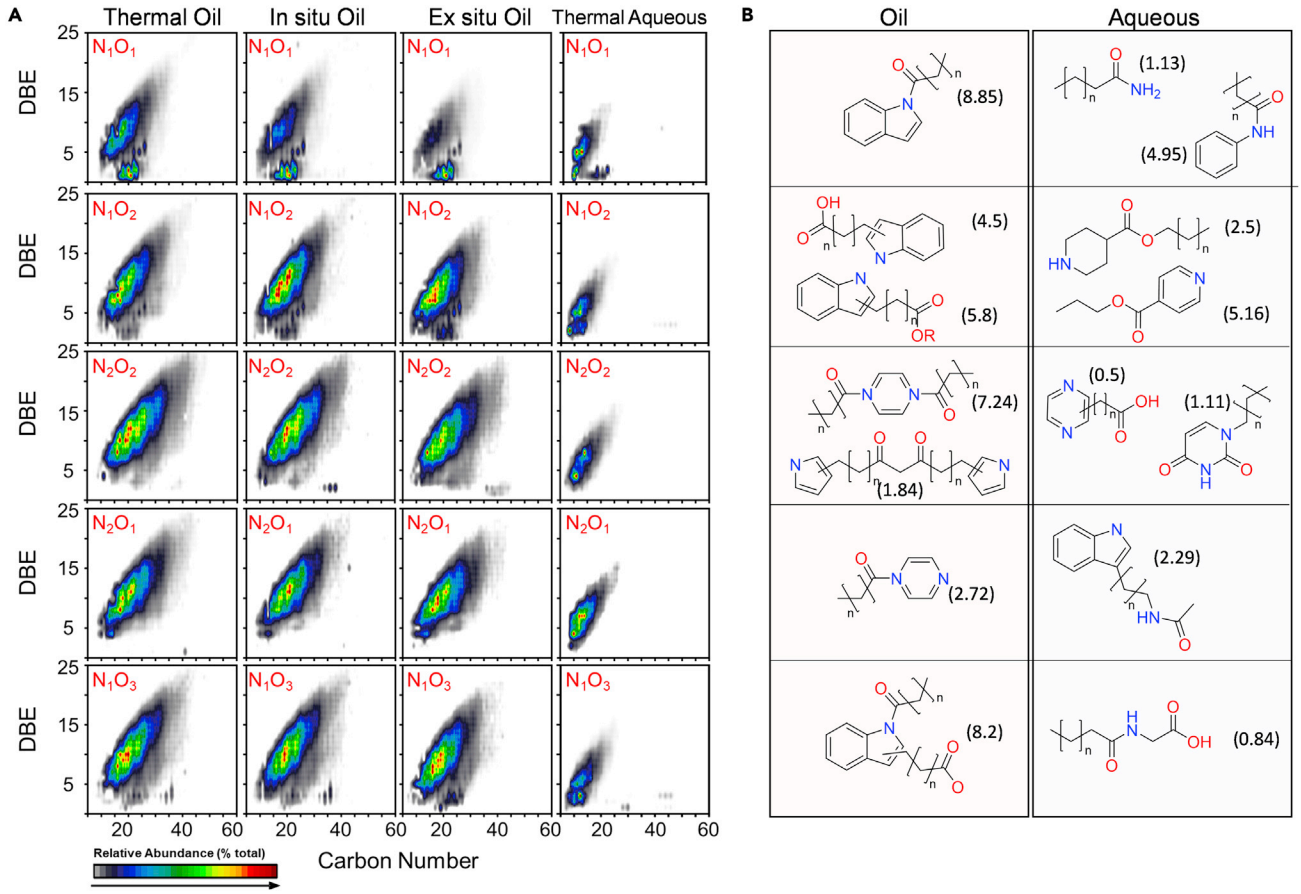


**Figure 4. FT-ICR MS analysis of HTL aqueous and biocrude products**

(A) Double-bond equivalency (DBE) as a function of carbon number for the five most abundant classes identified in (+)APPI FT-ICR MS for the three biocrude phases and the non-catalytic aqueous phase.

(B) Proposed molecular structures and classes consistent with regions of high abundance identified in part a for each heteroatom class. Numbers in parentheses indicate $K_{OW}$ for that particular molecule at that carbon number. See also Figure S14.

showing re-plots of the data shown in Figure 5 as relative abundance that shows compositional dependence in more detail.

The molecular weight distribution consists of several broad maxima, centered at 300, 450, and 600 Da. The first of these features is consistent with the fatty indoles identified from the analysis shown in Figure 4. The others, therefore, arise from further condensation reactions, including indoles with multiple fatty acid constituents and fatty acids cross-linked between indole groups. These molecular weight distributions are only weakly dependent on the presence or absence of catalyst, indicating that biocrude composition depends most strongly on the composition of the feed and secondarily on differences in formation conditions. Similarly, Figure 5 supports the conclusion that the main impact of catalysts is to produce greater amounts of biocrude forming molecules, without introducing entirely new molecules and hence without introducing new pathways and instead amplifying existing ones.

In addition to biocrude analysis, Figure 4 provides data obtained from analysis of the HTL aqueous phase. As expected from all previous discussion, for a given heteroatom class the aqueous phase product consists of lower carbon number and DBE than the same heteroatom class in the biocrude. The final column of Figure 4B provides molecular structures consistent with the aqueous phase FT-ICR MS data and previous reports of aqueous phase constituents (Chang et al., 2019; Mettler et al., 2012a, 2012b; Obeid et al., 2020). As compared with the biocrude phase, the aqueous phase consists of similar structural motifs, but with shorter fatty acid side chains that result in $K_{ow}$ values favoring aqueous phase partitioning rather than biocrude formation.

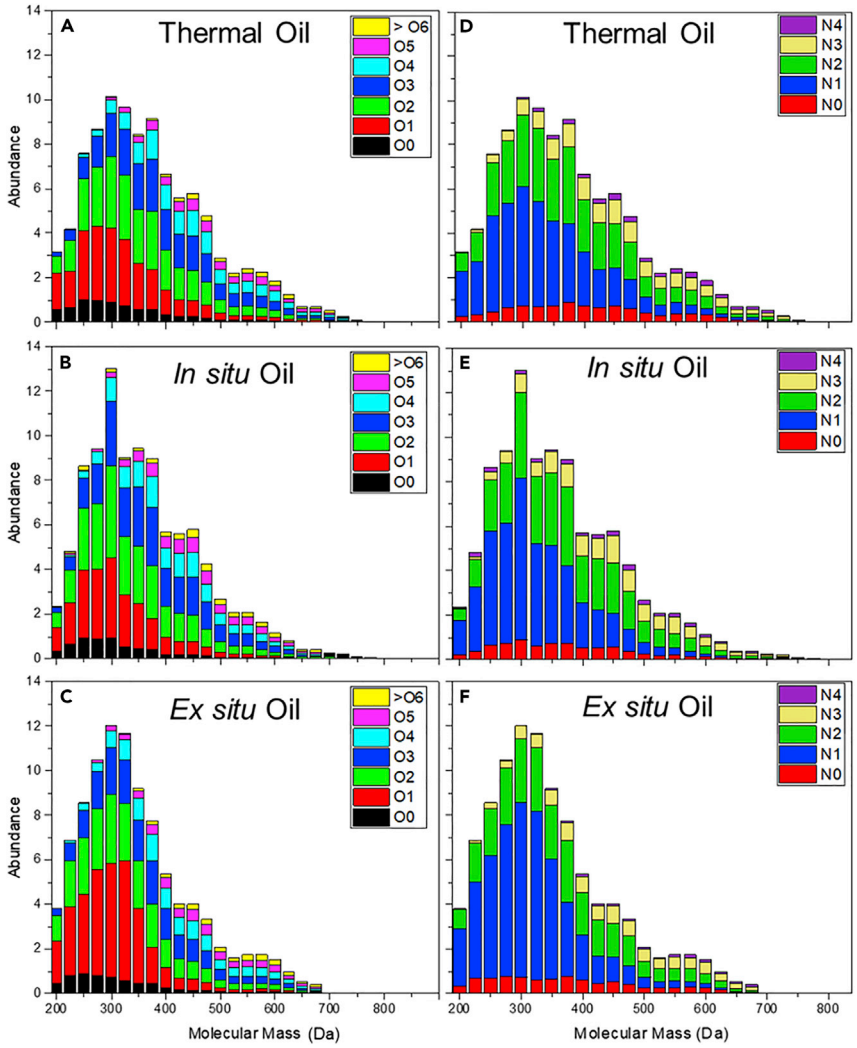


**Figure 5. Molecular weight distribution for oxygen and nitrogen-containing molecular classes derived from FT-ICR MS**

Relative abundance of different heteroatom classes as a function of molecular weight as determined by FT-ICR MS operating in (+) APPI mode.

(A–C) show data for oxygen bearing molecules and (D–F) show the same data for nitrogen bearing molecules. See also Figure S15.

Combining GC×GC and FT-ICR MS provides a detailed picture of the biocrude formed during HTL of food waste. Figure 6 is a schematic that captures the most important molecular details. Hydrolysis and thermolysis of the proteins, lipids, and starch present in food waste gives rise to amino acids, fatty acids, and simple carbohydrates. The $K_{ow}$ values of the fatty acids are sufficient for biocrude formation yet the amino acids and carbohydrates must undergo further dehydration and coupling reactions for biocrude formation. A critical step is formation of C-N and C-C bonds between the indole and phenol products of amino acid and carbohydrate degradation reactions to form fatty indoles that greatly increase the biocrude yield. These coupling reactions are responsible for biocrude yields that far exceed those predicted from the lipid content of the feed. The role of the acid-base catalyst is to boost these C-N and C-C forming reactions, thereby increasing the yields of these specific compounds while only secondarily impacting their structures.

Figure 6 provides $K_{ow}$ values for the various compounds identified in the biocrude. Based on appearance of compounds in the aqueous phase and biocrude phase, a value of $\log(K_{ow}) > 10$ is required for biocrude formation. This observation suggests a correlation between $K_{ow}$ and the corresponding biocrude-water

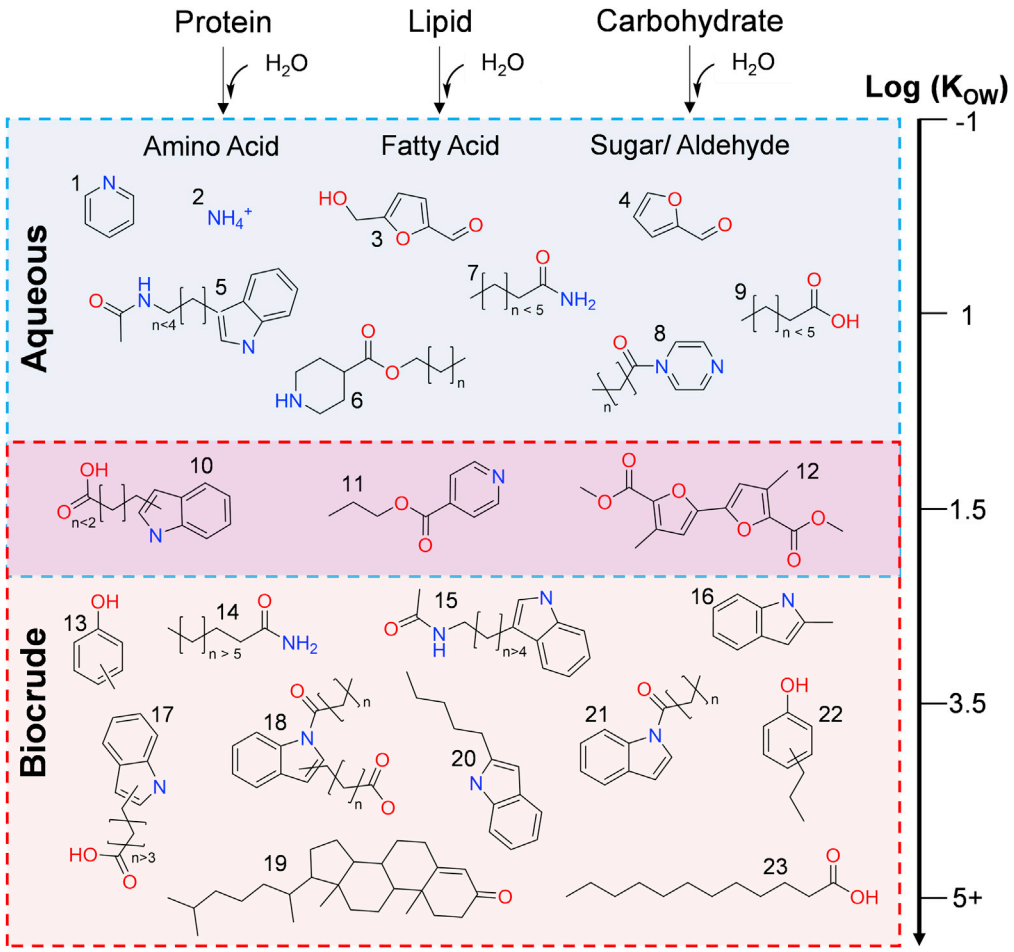


**Figure 6. Proposed schematic combining GC×GC and FT-ICR MS techniques for biocrude and aqueous partitioning**

Schematic representation of the molecules present in HTL liquid-phase products (biocrude and aqueous). Biocrude formation is the result of biopolymer hydrolysis and thermolysis followed by recombination. For food waste, formation of fatty indoles and alkyl phenols is especially important. $K_{ow}$ values are provided for the various compounds, showing that $\log(K_{ow}) > 2$ is required for biocrude formation.

partition coefficient ($K_{bw}$): $\log K_{bw} = \log K_{ow} + 1$. This correlation will be somewhat sensitive to the feedstock and to the reaction mixture pH, because many of the molecules present in the biocrude are ionizable acids, amines, or amides.

## Potential commercial impacts

Economic and environmental analyses were performed to evaluate the potential impacts of the new catalytic HTL technology for converting food waste into fuels. Environmental analysis included greenhouse gas (GHG) emissions reduction, which is provided in the main text, and impacts of secondary products (Figure S16). Economic analysis used a previous report by Pacific Northwest National Laboratory (PNNL) as a starting point that included detailed analysis of both capital and operating expenses (Snowden-Swan et al., 2016).

Full analysis of GHG reduction included three main components: $CO_2$ offsets due to replacing petroleum fuels with a renewable option, $CO_2$ emissions associated with refining food waste to diesel relative to those expected for converting petroleum to diesel, and reduction of GHG emissions due to re-directing food waste from landfills to use as a fuel.

Hydrotreating experiments, summarized in the Supporting Information (Figure S17), suggest hydrotreated biocrude obtained from food waste is suitable for use as a diesel blend stock or replacement and literature

**Table 2. Life cycle assessment emissions and resources calculations from GREET model of hydrothermal liquefaction**

| | Conventional Diesel | Diesel from Algae HTL (Ryan Davis et al., 2016, 2018) | Diesel from food HTL (base case) | Diesel from food HTL (+HAP-1.87) |
|---|---|---|---|---|
| Emissions (per MBTU) | | | | |
| Total $CO_2$ [kg] | 13.1 | 21.0 | 30.6 | 13.4 |
| CO [g] | 13.2 | 13.2 | 50.2 | 13.5 |
| $NO_x$ [g] | 23.5 | 24.9 | 63.8 | 23.3 |
| $PM_{10}$ [g] | 1.5 | 3.1 | 2.9 | 1.0 |
| $SO_x$ [g] | 7.5 | 86.8 | 29.5 | 10.8 |
| $CH_4$ [g] | 100 | 83.4 | 210 | 78.1 |
| Resources | | | | |
| Energy [MJ] | 1249 | 1506 | 1703 | 625 |

The life cycle of the catalyst is not specifically included in calculations due to the ability to use calcium and phosphorus as a soil amendment. See also Figure S18 and Table S4.

reports carbon recovery of nearly 70% (Castello et al., 2018; Cordova et al., 2020; Glaser and Lehr, 2019). Based on annual food waste production solely in the US (63 million tons) with an organic content of 25 wt% (Agency, 2021b; Zhang et al., 2007), food waste HTL has the potential to replace 4.5 million tons of diesel per year (28% of US diesel market) (Administration, 2021c), given that combustion of the food waste-derived diesel does not introduce new carbon into the atmosphere (i.e., $CO_2$ released by combustion will be taken up on rapid time scales to generate new food) and that combustion of petroleum diesel results in transfer of 3,082 kg of $CO_2$/ton of diesel from geological reserves to the atmosphere means that converting food waste to diesel has the potential to offset up to 15.3 million tons of $CO_2$ per year.

Converting food waste to diesel requires energy inputs. A well-to-pump life cycle analysis (Table 2) was performed using GREET software (Frank et al., 2011) to quantify the $CO_2$ emissions and energy input required for catalytic and non-catalytic HTL of food waste compared with petroleum-based diesel. LCA inputs (Figure S18, Table S4) are consistent with the flow rates and product usage identified in the technoeconomic analysis (TEA) (Hao Cai et al., 2013;Han et al., 2011; Lampert et al., 2015; Lu et al., 2018; Palou-Rivera and Wang, 2010). Of interest, producing diesel from food waste without a catalyst results in co-production of 2.3-times more $CO_2$ (30.6 tons) than producing diesel from petroleum (13.1 tons), a consequence of the low biocrude yield. Catalytic HTL of food waste results in $CO_2$ production values that are roughly equal to those for diesel production from petroleum (13.4 vs. 13.1 tons). These values are comparable to those reported previously by Fortier et al., 2014, 2017 and Nie et al. (Nie and Bi, 2018) for algae and biomass feedstocks, respectively, and indicate that GHG emissions from converting food waste to diesel roughly offset the emissions expected for converting petroleum to diesel. Accordingly, the GHG term due to HTL diesel production was neglected in further analysis of total GHG reduction. Similarly, the Energy Return on Investment (EROI) estimated for production of diesel from food waste is only 0.81 in the absence of catalysts and increases to 2.42 for catalytic HTL, indicating twice the energy is produced than is consumed in the process.

The well-to-pump analysis summarized in Table 2 does not account for GHG reductions associated with redirecting food waste from landfills. For landfills lacking methane capture, food waste decomposes to produce greenhouse gases, particularly methane, which is 50 times more climate forcing than $CO_2$ (Agency, 2016). The US produced 63 million tons of food waste in 2018, and the EPA estimates the methane potential of anaerobic digestion of food waste is equivalent to an estimated 2.49 tons of $CO_2$ per ton of waste (Agency, 2020). The result is that landfilling food waste results in annual emission of 156.8 million tons of GHG per year, which is equivalent to 2.4% of annual GHG emissions in the US (Administration, 2021a). Diverting food waste from landfills to production of renewable fuel avoids these emissions entirely.

The landfill gas and petroleum diesel replacement analyses can be summed to arrive at a final value for GHG reductions that can be expected from complete conversion of all US food waste into renewable diesel. The maximum possible reduction is 171 million tons/yr. This value is 2.6% of annual U.S. GHG emissions (Mausami Desai, 2021).While the assumptions of 100% of food waste collection and conversion to diesel is optimistic, this analysis provides a very reasonable first assessment of the magnitude of the

**Table 3. Predicted MFSP ($/GGE) for biocrude production from different feeds and HTL technologies**

| Feed | Feed Cost ($/dry ton) | Catalyst[b] | Catalyst Lifetime[c] (hrs) | Biocrude Yield (wt %) | MFSP[d] ($/GGE) | Source |
|---|---|---|---|---|---|---|
| Algae | 1171 | None | N/A | 40.9 | 11.35 | Jiang et al. (Jiang et al., 2019) |
| Algae | | | | 38.1 | 12.03 | |
| Algae | | | | 42.4 | 11.03 | |
| Food Waste | −45[a] | None | N/A | 13.6 | 8.24 | This work |
| | | HAP-1.57 | 100 | 32.1 | 8.54 | |
| | | HAP-1.86 | 200 | 31.8 | 6.11 | |
| | | HAP-1.86 alkali[e] | 200 | 40.7 | 4.78 | |

See also Tables S5–S7 and Figures S19 and 20.

[a]Feed cost includes transportation as $55/ton (Snowden-Swan et al., 2021).

[b]HAP catalysts were used with a catalyst cost of $11.34/lb. as found on Alibaba (2021a).

[c]Catalyst lifetime as determined experimentally.

[d]Minimum fuel selling price for biocrude without upgrading.

[e]Alkali costs taken as $330/metric ton = $0.01/lb. as found as Alibaba (2021b).

$CO_2$ reduction that is possible using the food waste to diesel strategy. Further LCA considerations as they pertain to HTL byproducts are discussed in the Supporting Information.

The LCA indicates the potential for positive environmental benefits of the new technology and clearly establishes the improvements that use of a catalyst can achieve. The next step was to analyze potential economic impacts by performing a TEA. Table S5 provides values of the inputs to this model (Snowden-Swan et al., 2016). A summary of the non-catalytic and catalytic TEA results can be found in Tables S6 and S7. To reflect current practice, a food waste tipping fee was included in the TEA and an aggregate average was calculated for tipping fees across the northeastern states of the USA (-$66.67) (Kantner, 2019) plus a fixed cost of $55/ton for transportation of the food waste to the HTL processing center.

Table 3 provides estimated values of the minimum fuel selling price (MFSP) of biocrude produced from food waste conversion using the catalytic HTL technology compared with similar values reported for an algae feedstock (Jiang et al., 2019; Snowden-Swan et al., 2016). Producing biocrude from algae results in an estimated MFSP >$10 per gallon of gasoline equivalent (GGE) (Jiang et al., 2019). The uncompetitive MFSP calculated for algae ($11.03) is a direct consequence of the high feedstock cost (>$1,000/ton) despite the high biocrude yield (40%) achievable with HTL processing of algae.

In the absence of catalyst, HTL conversion of food waste decreases MFSP ($8.24) by 28% relative to the average value predicted for algae. This reduction is a consequence of the tipping fee that can be claimed by processing food waste, despite the differences in biocrude yields obtained by the two processes (i.e., 13.6% compared with as much as 42.4%). Use of a catalyst to increase biocrude yield further decreases the estimated MFSP, with combined use of the heterogeneous-homogeneous catalyst described here resulting in a 57% reduction in MFSP ($4.78) relative to that estimated for algae without a catalyst. The added cost of the catalyst was more than offset by the biocrude yield improvements.

Sensitivity analysis indicated that tipping fees, catalyst cost and lifetime, and biocrude yields are the most important for determining MFSP, as summarized in Figures S19 and S20. Optimization of these parameters can realistically reduce the predicted MFSP of food waste biocrude. In particular, a tipping fee of −$45/ton, assuming a 50% moisture content, including transportation costs, is a conservative estimate (Snowden-Swan et al., 2021). Tipping fees are generally increasing across the USA, and tipping fees in Alaska already exceed $150/ton (Kantner, 2019), a value which corresponds to a predicted biocrude MFSP of $2.17/GGE for HAP-1.86 with alkali addition, even after including a reasonable estimate for transportation costs at $55/ton (Snowden-Swan et al., 2021).

Aside from deploying the technology in areas that maximize tipping fees, technological improvements can similarly reduce projected MFSP. The most easily validated area for reducing costs is extending the catalyst lifetime parameter input to the model. A 200 h catalyst lifetime used is a conservative estimate, since the

200 h endurance test was the longest test performed in this study. Varying the catalyst lifetime input to the model from 200 to 500 h results in a predicted MFSP of $3.56; a lifetime of 1,000 h results in an MFSP of $3.16. Further improvements in biocrude yield and/or decreased catalyst cost can have similar effects as extending the catalyst lifetime (Cheng et al., 2020, 2021).

Table 3 reflects only the MFSP projected for production of biocrude. However, refining the biocrude to a transportation fuel can earn renewable fuel incentives (Greene, 2017) for economically competitive production of HTL diesel. Previous analysis suggests that upgrading algae and sludge-derived HTL biocrude to diesel costs approximately $1.10/GGE (Snowden-Swan et al., 2016, 2021). Upgrading experiments performed on the food waste HTL biocrude show similar conversion of biocrude to diesel with 70% yield is possible using inexpensive molybdenum-based catalysts. The Supporting Information provides more detail on the upgrading experiments. Combining the most generous tipping fee currently reported in the USA ($150/wet ton) with modest extension of catalyst lifetime from 200 to 500 h, and the historical value of the renewable fuel credit appropriate for upgraded HTL diesel ($1.00/GGE) (Agency, 2021a; Greene, 2017) results in an estimated MFSP of $0.96/GGE for the HAP-1.86 + alkali biocrude (without incentives) and $1.06/GGE for the upgraded HTL diesel (including incentives) (Agency, 2021a; Greene, 2017). The projected values of the HTL diesel MFSP show that combining tipping fees, technological improvements, and renewable fuel credits provides a clear pathway for catalytic HTL conversion of food waste from a GHG emitting liability to an economically competitive renewable fuel.

### Limitations of the study

The economic analysis is based on the $n^{th}$ generation plant assumption and does not capture costs for an initial deployment. Environmental analysis through a life cycle assessment (LCA) utilizes assumptions about the efficiency of certain portions of the fuel production process, including those for obtaining the necessary electricity. Additionally, upgrading costs are currently based on experimental and model predictions from Pacific Northwest National Laboratory, and have the potential to change, both positively and negatively, depending on biocrude composition and catalyst choice. A single feedstock was used for all experiments and the current approach should be applied to a wider range of feeds to generalize the results observed here.

## STAR★METHODS

Detailed methods are provided in the online version of this paper and include the following:

- KEY RESOURCES TABLE
- RESOURCE AVAILABILITY
  - Lead contact
  - Materials availability
  - Data and code availability
- METHOD DETAILS
  - Food waste hydrothermal liquefaction
  - HTL product analysis
  - Catalyst characterization
  - Life cycle assessment and technoeconomic analysis
  - $CO_2$ and $NH_3$-TPD
  - Two-dimensional gas chromatography
  - Positive-ion APPI FT-ICR MS at 9.4 tesla

## SUPPLEMENTAL INFORMATION

Supplemental information can be found online at https://doi.org/10.1016/j.isci.2022.104916.

## ACKNOWLEDGMENTS

This work was funded by the DOE Bioenergy Technology Office (DE-EE0008513), a DOE DBIR (DE-SC0015784) and the MassCEC. The authors thank WenWen Yao, Department of Environmental Science at WPI, for TOC analysis, Mainstream Engineering for heating value characterization of the oil and solid samples, Wei Fan for assistance in obtaining SEM images and, Julia Martin and Ronald Grimm for their assistance in collecting XPS data, and Jeffrey R. Page for his assistance with oil upgrading and analysis.

HOL was partially funded for this work by NSF Graduate Research Fellowship award number 2038257. A portion of this work was performed at the National High Magnetic Field Laboratory Ion Cyclotron Resonance user facility, which is supported by the NSF Division of Materials Research and Division of Chemistry through DMR 16-44779 and the State of Florida.

## AUTHOR CONTRIBUTIONS

H.O.L. – conceptualization, investigation, formal analysis, writing – original draft and visualization. G.A.T. – methodology, investigation, writing – review and editing. A.D.P. – resources, data curation, writing – review and editing. A.M.M. and S.F.N. – resources, data curation, formal analysis, writing – review and editing. C.M.R. and R.K.N. – resources, data curation, formal analysis, writing – review and editing. F.C. – data curation and formal analysis. A.R.T. – conceptualization, visualization, writing – review and editing, supervision. M.T.T. – conceptualization, visualization, writing – review and editing, supervision, funding acquisition.

## DECLARATION OF INTERESTS

M.T.T and G.A.T. have a US patent on HTL technology (#11,286,432).

## INCLUSION AND DIVERSITY

While citing references scientifically relevant for this work, we also actively worked to promote gender balance in our reference list. The author list of this paper includes contributors from the location where the research was conducted who participated in the data collection, design, analysis, and/or interpretation of the work.

Received: March 21, 2022
Revised: April 25, 2022
Accepted: August 6, 2022
Published: August 31, 2022

## REFERENCES

Administration, U.S.E.I. (2021). Diesel Fuel Explained. https://www.eia.gov/energyexplained/diesel-fuel/.

Administration, U.S.E.I. (2021). Electricity Explained: Use of Electricity (Administration, U. S. E. I.).

Administration, U.S.E.I. (2021). Monthly Energy Review: August 2021 (Administration, U. S. E. I.).

Agency, E.P. (2016). Municipal Solid Waste (Agency, E. P).

Agency, E.P. (2020). Understanding Global Warming Potentials (Agency, E. P.).

Agency, E.P. (2021a). RIN Trades and Price Information (Agency, E. P.).

Agency, U.S.E.P. (2021b). Food: Material-specific Data. Facts and Figures about Materials, Waste and Recycling (Agency, U. S. E. P.).

Alibaba (2021a). Hydroxyapatite. https://www.alibaba.com/product-detail/Hydroxyapatite-Factory-Supply-Favorable-Price-Nano_1600292911748.html?.

Alibaba (2021). Sodium Hydroxide Flakes. https://www.alibaba.com/trade/search?fsb=y&IndexArea=product_en&CatId=80202&SearchText=sodium+hydroxide+50%25&viewtype=&tab=.

Azadi, P., and Farnood, R. (2011). Review of heterogeneous catalysts for sub- and supercritical water gasification of biomass and wastes. Int. J. Hydrogen Energy *36*, 9529–9541.

Besson, M., Gallezot, P., and Pinel, C. (2014). Conversion of biomass into chemicals over metal catalysts. Chem. Rev. *114*, 1827–1870.

Betancourt-Jimenez, D., Youngblood, J.P., and Martinez, C.J. (2020). Synthesis and characterization of fatty acid amides from commercial vegetable oils and primary alkyl amines for phase change material applications. ACS Sustain. Chem. Eng. *8*, 13683–13691.

Bielenberg, J., and Palou-Rivera, I. (2019). The RAPID Manufacturing Institute – reenergizing US efforts in process intensification and modular chemical processing. Chem. Eng. Process. *138*, 49–54.

Blakney, G.T., Hendrickson, C.L., and Marshall, A.G. (2011). Predator data station: a fast data acquisition system for advanced FT-ICR MS experiments. Int. J. Mass Spectrom. *306*, 246–252.

Budhwani, N. (2015). Removal of polycyclic aromatic hydrocarbons present in tyre pyrolytic oil using low cost natural adsorbents. Int. J. Biol. Biomol. Agric. Food Biotechnol. Eng. *9*, 186–190.

Castello, D., Pedersen, T., and Rosendahl, L. (2018). Continuous hydrothermal liquefaction of biomass: a critical review. Energies *11*, 3165.

Chang, H., Motagamwala, A.H., Huber, G.W., and Dumesic, J.A. (2019). Synthesis of biomass-derived feedstocks for the polymers and fuels industries from 5-(hydroxymethyl)furfural (HMF) and acetone. Green Chem. *21*, 5532–5540.

Cheng, F., Cui, Z., Chen, L., Jarvis, J., Paz, N., Schaub, T., Nirmalakhandan, N., and Brewer, C.E. (2017). Hydrothermal liquefaction of high- and low-lipid algae: bio-crude oil chemistry. Appl. Energy *206*, 278–292.

Cheng, F., Tompsett, G.A., Fraga Alvarez, D.V., Romo, C.I., Mckenna, A.M., Niles, S.F., Nelson, R.K., Reddy, C.M., Granados-Fócil, S., Paulsen, A.D., et al. (2021). Metal oxide supported Ni-impregnated bifunctional catalysts for controlling char formation and maximizing energy recovery during catalytic hydrothermal liquefaction of food waste. Sustain. Energy Fuels *5*, 941–955.

Cheng, F., Tompsett, G.A., Murphy, C.M., Maag, A.R., Carabillo, N., Bailey, M., Hemingway, J.J., Romo, C.I., Paulsen, A.D., Yelvington, P.E., and Timko, M.T. (2020). Synergistic effects of inexpensive mixed metal oxides for catalytic hydrothermal liquefaction of food wastes. ACS Sustain. Chem. Eng. *8*, 6877–6886.

Cordova, L.T., Lad, B.C., Ali, S.A., Schmidt, A.J., Billing, J.M., Pomraning, K., Hofstad, B., Swita, M.S., Collett, J.R., and Alper, H.S. (2020). Valorizing a hydrothermal liquefaction aqueous phase through co-production of chemicals and lipids using the oleaginous yeast Yarrowia lipolytica. Bioresour. Technol. *313*, 123639.

Corilo, Y.E. (2014). PetroOrg Software (Florida State University, Omics LLC).

Du, S., Valla, J.A., and Bollas, G.M. (2013). Characteristics and origin of char and coke from fast and slow, catalytic and thermal pyrolysis of biomass and relevant model compounds. Green Chem. *15*, 3214–3229.

EPA, U.S. (2020). U.S. Food Waste Statistics (EPA, U. S.).

Frank, E.D., Han, J., Palou-Rivera, I., Elgowainy, A., and Wang, M.Q. (2011). Life-Cycle Analysis of Algal Lipid Fuels with the GREET Model (Argonne National Laboratory GREET Publications).

Fihri, A., Len, C., Varma, R.S., and Solhy, A. (2017). Hydroxyapatite: a review of syntheses, structure and applications in heterogeneous catalysis. Coord. Chem. Rev. *347*, 48–76.

Fortier, M.-O.P., Roberts, G.W., Stagg-Williams, S.M., and Sturm, B.S. (2014). Life cycle assessment of bio-jet fuel from hydrothermal liquefaction of microalgae. Appl. Energy *122*, 73–82.

Fortier, M.-O.P., Roberts, G.W., Stagg-Williams, S.M., and Sturm, B.S. (2017). Determination of the life cycle climate change impacts of land use and albedo change in algal biofuel production. Algal Res. *28*, 270–281.

Glaser, B., and Lehr, V.-I. (2019). Biochar effects on phosphorus availability in agricultural soils: a meta-analysis. Sci. Rep. *9*, 9338.

Gollakota, A., and Savage, P.E. (2020). Fast and isothermal hydrothermal liquefaction of polysaccharide feedstocks. ACS Sustain. Chem. Eng. *8*, 3762–3772.

Gollakota, A.R.K., Kishore, N., and Gu, S. (2018). A review on hydrothermal liquefaction of biomass. Renew. Sustain. Energy Rev. *81*, 1378–1392.

Greene, P. (2017). 101 for RINs. (BioCycle: The organics recycling authority). https://www.biocycle.net/101-for-rins/.

Hao Cai, J.H., Grant Forman, V.D., Elgowainy, A., and Wang, M. (2013). Analysis of Petroleum Refining Energy Efficiency of U.S. Refineries (Argonne National Lab Database).

He, C., Fang, Z., Li, Y., Jiang, C., Zhao, S., Xu, C., Zhang, Y., and Shi, Q. (2021). Ionization selectivity of electrospray and atmospheric pressure photoionization FT-ICR MS for petroleum refinery wastewater dissolved organic matter. Environ. Sci. Process. Impacts *23*, 1466–1475.

Hu, H.-S., Wu, Y.-L., and Yang, M.-D. (2018). Fractionation of bio-oil produced from hydrothermal liquefaction of microalgae by liquid-liquid extraction. Biomass Bioenergy *108*, 487–500.

Hughey, C.A., Hendrickson, C.L., Rodgers, R.P., Marshall, A.G., and Qian, K. (2001). Kendrick mass defect spectrum: a compact visual analysis for ultrahigh-resolution broadband mass spectra. Anal. Chem. *73*, 4676–4681.

Han, J., Mintz, M., and Wang, M.Q. (2011). Waste-to-Wheel Analysis of Anaerobic-Digestion-Based Renewable Natural Gas Pathways with the GREET Model (Argonne National Laboratory).

Jiang, Y., Jones, S.B., Zhu, Y., Snowden-Swan, L., Schmidt, A.J., Billing, J.M., and Anderson, D. (2019). Techno-economic uncertainty quantification of algal-derived biocrude via hydrothermal liquefaction. Algal Res. *39*, 101450.

Kantner, D.L. (2019). Analysis of MSW Landfill Tipping Fees (Environmental Research & Education Foundation).

Kaiser, N.K., Quinn, J.P., Blakney, G.T., Hendrickson, C.L., and Marshall, A.G. (2011a). A novel 9.4 tesla FTICR mass spectrometer with improved sensitivity, mass resolution, and mass range. J. Am. Soc. Mass Spectrom. *22*, 1343–1351.

Kaiser, N.K., Savory, J.J., Mckenna, A.M., Quinn, J.P., Hendrickson, C.L., and Marshall, A.G. (2011b). Electrically compensated fourier transform ion cyclotron resonance cell for complex mixture mass analysis. Anal. Chem. *83*, 6907–6910.

Kaneda, K., Mori, K., Hara, T., Mizugaki, T., and Ebitani, K. (2004). Design of hydroxyapatite-bound transition metal catalysts for environmentally-benign organic syntheses. Catal. Surv. Asia *8*, 231–239.

Kendrick, E. (1963). A mass scale based on CH2 = 14.0000 for high resolution mass spectrometry of organic compounds. Anal. Chem. *35*, 2146–2154.

Kiani, D., and Baltrusaitis, J. (2021). Surface chemistry of hydroxyapatite for sustainable n-butanol production from bio-ethanol. Chem Catalysis *1*, 782–801.

Kumar, S., Lange, J.-P., Van Rossum, G., and Kersten, S.R. (2015). Bio-oil fractionation by temperature-swing extraction: principle and application. Biomass Bioenergy *83*, 96–104.

Lampert, D.J., Cai, H., Wang, Z., Keisman, J., Wu, M., Han, J., Dunn, J., Sullivan, J.L., Elgowainy, A., Wang, M., and Keisman, J. (2015). Development of a Life Cycle Inventory of Water Consumption Associated with the Production of Transportation Fuels (US Department of Energy). https://doi.org/10.2172/1224980.

Lamping, M., Enck, S., and Geyer, A. (2015). Inverse γ-turn-inspired peptide: synthesis and analysis of segetalin A indole hemiaminal. Eur. J. Org. Chem. *2015*, 7443–7448.

Lu, J., Li, H., Zhang, Y., and Liu, Z. (2018). Nitrogen migration and transformation during hydrothermal liquefaction of livestock manures. ACS Sustain. Chem. Eng. *6*, 13570–13578.

Lucian, M., Volpe, M., Gao, L., Piro, G., Goldfarb, J.L., and Fiori, L. (2018). Impact of hydrothermal carbonization conditions on the formation of hydrochars and secondary chars from the organic fraction of municipal solid waste. Fuel *233*, 257–268.

Maag, A., Paulsen, A., Amundsen, T., Yelvington, P., Tompsett, G., and Timko, M. (2018). Catalytic hydrothermal liquefaction of food waste using CeZrOx. Energies *11*, 564.

Mausami Desai, V.C. (2021). Inventory of U.S. Greenhouse Gas Emissions and Sinks (Agency, U. S. E. P.).

Mclafferty, F.W., and Turecek, F. (1993). Interpretation of Mass Spectra, Fourth edition (University Science Books).

Meshram, H.M., Thakur, P.B., and Bejjam, M.B. (2013). An efficient synthesis of hemiaminal of indoles by using tetrabutylammonium fluoride (TBAF) in water as a reusable reaction media. Green Chem. Lett. Rev. *6*, 95–100.

Mettler, M.S., Mushrif, S.H., Paulsen, A.D., Javadekar, A.D., Vlachos, D.G., and Dauenhauer, P.J. (2012a). Revealing pyrolysis chemistry for biofuels production: conversion of cellulose to furans and small oxygenates. Energy Environ. Sci. *5*, 5414–5424.

Mettler, M.S., Vlachos, D.G., and Dauenhauer, P.J. (2012b). Top ten fundamental challenges of biomass pyrolysis for biofuels. Energy Environ. Sci. *5*, 7797–7809.

Meylan, W.M., Howard, P.H., and Boethling, R.S. (1996). Improved method for estimating water solubility from octanol/water partition coefficient. Environ. Toxicol. Chem. *15*, 100–106.

Mostafa, N.Y. (2005). Characterization, thermal stability and sintering of hydroxyapatite powders prepared by different routes. Mater. Chem. Phys. *94*, 333–341.

Nagappan, S., Bhosale, R.R., Nguyen, D.D., Chi, N.T.L., Ponnusamy, V.K., Woong, C.S., and Kumar, G. (2021). Catalytic hydrothermal liquefaction of biomass into bio-oils and other value-added products – a review. Fuel *285*, 119053.

Nie, Y., and Bi, X. (2018). Life-cycle assessment of transportation biofuels from hydrothermal liquefaction of forest residues in British Columbia. Biotechnol. Biofuels *11*, 23.

Obeid, R., Lewis, D.M., Smith, N., Hall, T., and Van Eyk, P. (2020). Reaction kinetics and characterisation of species in renewable crude from hydrothermal liquefaction of monomers to represent organic fractions of biomass feedstocks. Chem. Eng. J. *389*, 124397.

Ouadi, M., Bashir, M.A., Speranza, L.G., Jahangiri, H., and Hornung, A. (2019). Food and market waste–A pathway to sustainable fuels and waste valorization. Energy Fuels *33*, 9843–9850.

Palou-Rivera, I., and Wang, M.Q. (2010). Updated Estimation of Energy Efficiencies of U.S. Petroleum Refineries (US Department of Energy). https://doi.org/10.2172/1009352.

Paritosh, K., Kushwaha, S.K., Yadav, M., Pareek, N., Chawade, A., and Vivekanand, V. (2017). Food waste to energy: an overview of sustainable approaches for food waste management and nutrient recycling. Biomed. Res. Int. *2017*, 2370927.

Peterson, A.A., Vogel, F., Lachance, R.P., Fröling, M., Antal, M.J., Jr., and Tester, J.W. (2008). Thermochemical biofuel production in hydrothermal media: a review of sub- and supercritical water technologies. Energy Environ. Sci. *1*, 32–65.

Pfaltzgraff, L.A., De Bruyn, M., Cooper, E.C., Budarin, V., and Clark, J.H. (2013). Food waste biomass: a resource for high-value chemicals. Green Chem. *15*, 307–314.

Purcell, J.M., Hendrickson, C.L., Rodgers, R.P., and Marshall, A.G. (2006). Atmospheric pressure photoionization fourier transform ion cyclotron resonance mass spectrometry for complex mixture analysis. Anal. Chem. *78*, 5906–5912.

Purcell, J.M., Hendrickson, C.L., Rodgers, R.P., and Marshall, A.G. (2007a). Atmospheric pressure photoionization proton transfer for complex organic mixtures investigated by Fourier transform ion cyclotron resonance mass spectrometry. J. Am. Soc. Mass Spectrom. *18*, 1682–1689.

Purcell, J.M., Rodgers, R.P., Hendrickson, C.L., and Marshall, A.G. (2007b). Speciation of nitrogen containing aromatics by atmospheric pressure photoionization or electrospray ionization Fourier transform ion cyclotron resonance mass spectrometry. J. Am. Soc. Mass Spectrom. *18*, 1265–1273.

Robb, D.B., and Blades, M.W. (2006). Factors affecting primary ionization in dopant-assisted atmospheric pressure photoionization (DA-APPI) for LC/MS. J. Am. Soc. Mass Spectrom. *17*, 130–138.

Robb, D.B., Covey, T.R., and Bruins, A.P. (2000). Atmospheric pressure photoionization: an ionization method for liquid chromatography–mass spectrometry. Anal. Chem. *72*, 3653–3659.

Roberts, G.W., Sturm, B.S.M., Hamdeh, U., Stanton, G.E., Rocha, A., Kinsella, T.L., Fortier, M.-O.P., Sazdar, S., Detamore, M.S., and Stagg-Williams, S.M. (2015). Promoting catalysis and high-value product streams by in situ hydroxyapatite crystallization during hydrothermal liquefaction of microalgae cultivated with reclaimed nutrients. Green Chem. *17*, 2560–2569.

Ryan Davis, A.C., Wigmosta, M., Markham, J., Kinchin, C., Zhu, Y., Jones, S., Han, J., Canter, C., and Li, Q. (2018). 2017 Algae Harmonization Study: Evaluating the Potential for Future Algal Biofuel Costs, Sustainability, and Resource Assessment from Harmonized Modeling (Argonne National Laboratory, National Renewable Energy Laboratory, Pacific Northwest National Laboratory).

Ryan Davis, J.M., Kinchin, C., Grundl, N., Eric, C., and Tan, D. (2016). Process Design and Economics for the Production of Algal Biomass: Algal Biomass Production in Open Pond Systems and Processing Through Dewatering for Downstream Conversion (Energy, U. S. D. O).

Sad, M.E., Padró, C., and Apesteguía, C. (2008). Selective synthesis of p-cresol by methylation of phenol. Appl. Catal. Gen. *342*, 40–48.

Sangster, J. (1989). Octanol-water partition coefficients of simple organic compounds. J. Phys. Chem. Ref. Data *18*, 1111–1229.

Savory, J.J., Kaiser, N.K., Mckenna, A.M., Xian, F., Blakney, G.T., Rodgers, R.P., Hendrickson, C.L., and Marshall, A.G. (2011). Parts-per-billion fourier transform ion cyclotron resonance mass measurement accuracy with a "walking" calibration equation. Anal. Chem. *83*, 1732–1736.

Schanes, K., Dobernig, K., and Gözet, B. (2018). Food waste matters - a systematic review of household food waste practices and their policy implications. J. Clean. Prod. *182*, 978–991.

Senko, M.W., Hendrickson, C.L., Emmett, M.R., Shi, S.D.H., and Marshall, A.G. (1997). External accumulation of ions for enhanced electrospray ionization fourier transform ion cyclotron resonance mass spectrometry. J. Am. Soc. Mass Spectrom. *8*, 970–976.

Simpson, R.B., Ashbrook, J.D., Santos, E.C., and Spector, A.A. (1974). Partition of fatty acids. J. Lipid Res. *15*, 415–422.

Smith, D.R., Robb, D.B., and Blades, M.W. (2009). Comparison of dopants for charge exchange ionization of nonpolar polycyclic aromatic hydrocarbons with reversed-phase LC-APPI-MS. J. Am. Soc. Mass Spectrom. *20*, 73–79.

Snowden-Swan, L.J., Zhu, Y., Jones, S.B., Elliot, D.C., Schmidt, A.J., Hallen, R.T., Billing, J.M., Hart, T.R., Fox, S., and Maupin, G.D. (2016). In Hydrothermal Liquefaction and Upgrading of Municipal Wastewater Treatment Plant Sludge: A Preliminary Techno-Economic Analysis (Energy, D. O.).

Snowden-Swan, L.J., Li, S., Jiang, Y., Thorson, M.R., Schmidt, A.J., Seiple, T., Billing, J.M., Santosa, D.M., Hart, T.R., Fox, S.P., et al. (2021). Wet Waste Hydrothermal Liquefaction and Biocrude Upgrading to Hydrocarbon Fuels: 2020 State of Technology (Pacific Northwest National Laboratory).

Stummann, M.Z., Høj, M., Davidsen, B., Hansen, L.P., Beato, P., Gabrielsen, J., Jensen, P.A., and Jensen, A.D. (2019). Deactivation of a CoMo catalyst during catalytic hydropyrolysis of biomass. Part 2. Characterization of the spent catalysts and char. Energy Fuels *33*, 12387–12402.

Tolmachev, A.V., Robinson, E.W., Wu, S., Kang, H., Lourette, N.M., Pasa-Tolić, L., and Smith, R.D. (2008). Trapped-ion cell with improved dc potential harmonicity for FT-ICR MS. J. Am. Soc. Mass Spectrom. *19*, 586–597.

Tsuchida, T., Kubo, J., Yoshioka, T., Sakuma, S., Takeguchi, T., and Ueda, W. (2008a). Reaction of ethanol over hydroxyapatite affected by Ca/P ratio of catalyst. J. Catal. *259*, 183–189.

Tsuchida, T., Sakuma, S., Takeguchi, T., and Ueda, W. (2006). Direct synthesis of n-butanol from ethanol over nonstoichiometric hydroxyapatite. Ind. Eng. Chem. Res. *45*, 8634–8642.

Tsuchida, T., Yoshioka, T., Sakuma, S., Takeguchi, T., and Ueda, W. (2008b). Synthesis of biogasoline from ethanol over hydroxyapatite catalyst. Ind. Eng. Chem. Res. *47*, 1443–1452.

Wan, S., and Wang, Y. (2014). A review on ex situ catalytic fast pyrolysis of biomass. Front. Chem. Sci. Eng. *8*, 280–294.

Wilcox, B.E., Hendrickson, C.L., and Marshall, A.G. (2002). Improved ion extraction from a linear octopole ion trap: SIMION analysis and experimental demonstration. J. Am. Soc. Mass Spectrom. *13*, 1304–1312.

Xian, F., Corilo, Y.E., Hendrickson, C.L., and Marshall, A.G. (2012). Baseline correction of absorption-mode Fourier transform ion cyclotron resonance mass spectra. Int. J. Mass Spectrom. *325–327*, 67–72.

Xian, F., Hendrickson, C.L., Blakney, G.T., Beu, S.C., and Marshall, A.G. (2010). Automated broadband phase correction of fourier transform ion cyclotron resonance mass spectra. Anal. Chem. *82*, 8807–8812.

Zhang, R., El-Mashad, H.M., Hartman, K., Wang, F., Liu, G., Choate, C., and Gamble, P. (2007). Characterization of food waste as feedstock for anaerobic digestion. Bioresour. Technol. *98*, 929–935.

Zissimos, A.M., Abraham, M.H., Barker, M.C., Box, K.J., and Tam, K.Y. (2002). Calculation of Abraham descriptors from solvent-water partition coeffcients in four different systems; evaluation of different methods of calculation. J. Chem. Soc. Perkin Trans. 2 *2*, 470–477.

## STAR★METHODS

### KEY RESOURCES TABLE

| REAGENT or RESOURCE | SOURCE | IDENTIFIER |
|---|---|---|
| Chemicals, peptides, and recombinant proteins | | |
| Hydroxyapatite | Sigma Aldrich | 677418 |
| Hydroxyapatite | Sigma Aldrich | 900195 |
| $Ca(NO_3)_2$ | Sigma Aldrich | C1396 |
| $(NH_4)_2HPO_4$ | Sigma Aldrich | A5764 |
| Acetone | Fisher Scientific | A18-4 |
| Nitrogen gas | Airgas | NI UHP300 |
| Helium gas | Airgas | He UHP300 |
| Software and algorithms | | |
| PetroOrg | National High Magnetic Field Laboratory, 2021 | https://nationalmaglab.org/user-facilities/icr/icr-software |
| MagicPlot | MagicPlot, 2020 | https://magicplot.com/index.php#download |

### RESOURCE AVAILABILITY

#### Lead contact

Further information and requests for resources and materials should be directed to and will be fulfilled by the lead contact, Michael Timko (mttimko@wpi.edu).

#### Materials availability

Synthesized HAP materials are available upon request. All FT-ICR MS spectra are provided via Open Science Framework https://osf.io/64bmt/ through https://doi.org/10.17605/OSF.IO/KNHA5.

#### Data and code availability

The datasets generated in this study are available by request from the lead contact.

### METHOD DETAILS

#### Food waste hydrothermal liquefaction

HTL experiments were conducted in a 300 mL stainless steel Parr reactor (Model 4561), fitted with a magnetic stirrer. For each experiment, 100 g of food waste slurry (15 wt % solids) was loaded into the reactor. All catalytic experiments were performed with 5 wt % catalyst, unless otherwise noted. After loading, the reactor was sealed and purged three times with nitrogen to remove residual air before pressurization to 65.5 $\pm$ 5 bar and heating to 300 $\pm$ 5°C at approximately 6°C/min using an external heating jacket. After heating, the reactor pressure was 200 $\pm$ 5 bar, sufficient to maintain water in its liquid state. The reaction temperature was maintained within $\pm$5°C of 300°C with an immersed Type K thermocouple and PID controller. After 60 min at 300°C, the reaction was quenched by placing the reactor in an ice bath until the measured temperature reached 38 $\pm$ 2°C. Quenching required less than 10 min.

All runs were completed in at least duplicate, with yield measurements agreeing to within $\pm$10% when experiments were performed under identical conditions. Average values obtained from these experiments are presented here. Error was calculated as the standard deviation between replicates of the same experimental conditions. For safety, the reactor setup was equipped with a pressure-relief valve and located in a fume-hood.

### HTL product analysis

Upon reaction quenching, HTL products partition into four phases (i.e., gas, aqueous, oil, and char) that can each be quantified, as reported previously (Cheng et al., 2020; Maag et al., 2018). The overall mass balance was determined by summing the individual product yields and was found to close within 10% for all experiments. Mass yields were derived from the organic concentration loaded into the reactor. Reactor losses represent residual material that could not be removed from the reactor, transfer losses, and the precision of the analytical balance used to estimate gas yields ($\pm$ 0.5 g).

Solid and liquid products were separated via vacuum filtration (Whatman no. 1 filter paper, 11μm). Oil products remained with the solid char on the filter while aqueous products were collected in the vacuum flask. Solid and oil products were then weighed and rinsed with approximately 1 L of acetone to separate and collect the oil before using a rotary evaporator at 50 $\pm$ 5°C and under vacuum (350 mmHg). The remaining solids containing spent catalyst and char were dried overnight and weighed before additional analysis. Char yield was calculated by subtracting the known mass of added catalyst from the total mass of solid product. For catalyst reuse experiments, the filtered solids were placed in a COORS USA ceramic boat and calcined in a quartz tube clam shell furnace at 550°C under continuous air flow (50 $cm^3$/min) for 6 h to combust char and recover the catalyst.

Elemental analysis (CHON) was performed on the food waste feedstock, oil, and char phases at Midwest Microlabs (Indianapolis, IN). The oil and feedstock were also sent to Mainstream Engineering for higher heating value (HHV) analysis using a semimicro calorimeter (25720, Parr, Moline, IL) calibrated with benzoic acid. Total organic carbon (TOC) content of the aqueous phase was measured using a TOC analyzer (Shimadzu, Kyoto, Japan). The samples were diluted and acidified with 1 μL of 6 M HCl per 1 mL of sample and conducted in duplicate. Product mass yields were then utilized in conjunction with elemental analysis, TOC, and gas-phase GC TCD to determine the resultant carbon mass balance (Equation 1).

$$Carbon\ Yield_{product} = \frac{C_{product} \times Mass_{product}\ (g)}{C_{feed} \times Mass_{feed}\ (g)} \quad \text{(Equation 1)}$$

Carbon mass balance was evaluated by summing the carbon present in the biocrude, char, aqueous, and gas phases. In all cases, the carbon mass balance closed to within 10%. Energy recovery was calculated to determine the amount of energy recovered as desired product as a function of the feedstock energy.

$$Energy\ Recovery = \frac{HHV_{oil} \times Mass_{oil}\ (g)}{HHV_{feed} \times Mass_{feed}} \quad \text{(Equation 2)}$$

Comprehensive two-dimensional gas chromatography was performed on the biocrudes as described in the SI. Fourier transform attenuated total reflection infrared spectroscopy (FT-ATR-IR) with a resolution of 8 $cm^{-1}$ was used with eight scans taken and averaged for each sample for all biocrude oils to understand biocrude functional groups.

### Catalyst characterization

The different types of HAP were characterized to quantify their surface area via $N_2$ sorption, acid and base site densities via $CO_2$ and $NH_3$ temperature programmed desorption (TPD), crystallinity through X-ray powder diffraction (XRD), elemental composition of the surface via X-ray photoelectron spectroscopy, and morphology via scanning electron microscopy (SEM).

### Life cycle assessment and technoeconomic analysis

The LCA was performed using the GREET software developed at Argonne National Laboratory. The diesel upgrading step was taken as pre-set in the software for HTL biocrude upgrading to renewable diesel II. A TEA was provided by Pacific Northwest National Laboratory as developed for their 2016 report on sewage sludge (Snowden-Swan et al., 2016). Cost, yield, and quality data were altered as shown in Table S5 to be representative of food waste and food waste experiments. The base PNNL model was modified to include a catalyst by adding the cost to the 'Simple Costs' tab on a per pound basis, and the lifetime included in HTL flows. HAP cost data was taken from Alibaba, where a price of $28.00/kg was utilized (Alibaba, 2021a). Food waste feedstock cost was assumed to have a tipping fee of-$66.53/wet ton, consistent with data published by the Environmental Research & Education Foundation (Kantner, 2019).

HAP catalyst was washed with deionized water (>18MΩ cm) utilizing centrifugation until the pH of the resultant water phase remained constant, occurring at pH = 7. Approximately 5g of HAP-1.86 was loaded into a centrifuge tube along with 40 mL of DI water. The mixture was shaken for 1 min before being placed in a centrifuge to separate the solid and liquid phases. The pH of the resultant liquid phase was measured before being discarded in a waste container. 40 mL of fresh DI water was then added to the remaining HAP, mixed again for 1 min and placed in the centrifuge. This process was repeated until the liquid pH remained unchanged for 2 cycles, which took on average 6 total cycles to achieve.

The catalyst crystallinity was determined by X-ray diffraction (XRD) before and after use in HTL. An X-ray powder diffractometer (Geigerflex, Rigaku Co., Tokyo, Japan) equipped with the Bragg-Brentano theta-theta configuration was used with CuKα radiation at 27.5 kV and 25 mA. Spectra were obtained in the range of 6–80° 2θ with a step size of 0.02°.

The morphology of fresh and spent catalysts was characterized using scanning electron microscopy (SEM). Ca/P ratios were determined through use of a PHI5600 X-ray photoelectron spectroscopy system equipped with a third-party data acquisition system (RBD Instruments, Bend, OR). Base chamber pressures remained below $5 \times 10^{-9}$ torr during all data acquisition. The photoelectrons were collected with a hemispherical energy analyzed positioned at 90° with respect to the incoming mono-chromated Al Kα X-radiation.

### $CO_2$ and $NH_3$-TPD

Nitrogen sorption was utilized to investigate the surface area distribution in all HAP samples examined. Nitrogen sorption is a bulk technique that takes into consideration the porosity of the entire sample. Below $P/P_0$ of $10^{-3}$ the isotherm can be associated with gas-catalyst interactions within micropores, whereas for $P/P_0$> 0.1 the isotherm is associated with mesopore gas-gas interactions. Acid and base site densities of the oxide catalysts were determined using NH3- and CO2- temperature programmed desorption (TPD) analysis, respectively. A Quantachrome Autosorb iQ adsorption/chemisorption system equipped with a thermal conductivity detector (TCD), was used for the TPD analysis. The TPD methods used were similar to those reported by Rodrigues et al. and Käßner et al. Samples were degassed under continuous flow of helium (20 cm3 min–1) at 550°C for 3 h, followed by cooling to 30°C. After degassing, samples were then saturated under CO2 gas flow for 10 min at 30°C, after which the sample cell was purged with helium for 30 min at 30°C to remove excess CO2. The CO2-adsorbed sample was then heated from 30 to 800°C at a heating rate of 10°C min–1 under helium, and the CO2 off-gas was quantified using a TCD detector. A similar method was used for NH3-TPD analysis to quantify acid sites. Samples were degassed under continuous helium flow for 120 min, cooled to 100°C, and the sample saturated under continuous NH3 flow for 10 min. Degassing temperatures were set based on the thermal stability of the material. After NH3 saturation, the sample cell was purged under continuous helium flow for 30 min, heated to 800°C at a rate of 2°C min−1, and finally flushed with helium for 30 min. The off-gas was continuously monitored by a TCD detector. TPD calibration curves were generated using a range of measured volumes of NH3 and CO2. The areas under the standard TPD curves were calculated using Magicplot software. The base and acid site densities were calculated as μmol g–1 using TCD response factors.

Surface properties were evaluated using $N_2$ adsorption at −196.15°C using a Quantachrome Autosorb iQ TPX instrument (Anton Paar Co., Graz, Austria). Before $N_2$ dosing, 500–1000 mg catalyst was degassed at 120°C for up to 3 h under vacuum. Total surface area was estimated by fitting measured isotherms using the using the Brunauer–Emmett–Teller (BET) method. Mesopore diameters were estimated using Barrett–Joyner–Halenda (BJH) method and the micropore volume and surface area using the Dubinin–Radushkevich (DR) method.

### Two-dimensional gas chromatography

GC×GC-FID chromatography methods were adapted from Cheng et al. (2021) as follows. Analyses were performed on a LECO GC×GC instrument equipped with an Agilent 7890A GC configured with a 7683B series split/splitless auto-injector. Biocrude samples dissolved in toluene were injected in splitless mode with a hydrogen carrier gas at 1mL $min^{-1}$. The cold jet utilized liquid nitrogen and the hot jet offset was 15°C above the temperature of the primary GC oven (inlet T = 310°C). The first dimension column was a Restek Rxi-1ms (60m, 0.25 mm ID, 0.25 μm df) whereas the second column was a 50% phenyl polysilphenylene-siloxane column (SGE BPX50, 1.2m, 0.10 mm ID, 0.1 μm df). The main oven was held at 65°C for 12.5 min before ramping from 50 to 340°C at a rate of 1.25°C$min^{-1}$. The second-dimension oven

temperature program was held at 70°C (12.5 min) before ramping to 345°C at 1.25°Cmin$^{-1}$. The hot jet pulse width was 1.0 s with a modulation period of 6.5 s with a 2.5 s cooling period. FID data was obtained with an acquisition rate of 100 data points per second.

GC×GC-HRT analysis was performed on a LECO Pegasus GC×GC-HRT 4D system equipped with an Agilent 7890A GC and configured with a LECO LPAL3 auto-injector and a LECO dual stage cryogenic modulator. Samples were injected in splitless mode with a helium carrier gas at 1 mLmin$^{-1}$. The cold jet utilized liquid nitrogen and the hot jet offset was 15°C above the temperature of the primary GC oven (inlet T = 310°C). The first dimension column was an SGE BPX-50 (60m, 0.25mm ID, 0.25μm df) with an SGE BPX-50 (2m, 0.25mm ID, 0.25μm df) second dimension column. The main oven was held at 80°C for 12.5 min before ramping from 80 to 330°C at a rate of 1.25°Cmin$^{-1}$. The hot jet pulse width was set at 2.0 s with an 8 s modulation period. The second-dimension oven temperature program was held at 85°C (12.5 min) before ramping to 335°C at 1.25°Cmin$^{-1}$. Mass resolution was +/− 0.0005 amu and sampled with an acquisition rate of 200 spectra per second in the mass range of 40–700 amu. The ionization method was EI with an electron energy of −70 V and an extraction frequency of 1.5 kHz.

### Positive-ion APPI FT-ICR MS at 9.4 tesla

Samples dissolved in toluene to a final concentration of 125 μg/mL for (+) atmospheric pressure photoionization Fourier transform ion cyclotron resonance mass spectrometry (APPI FT-ICR MS) at a flow rate of 50 μL/min (Purcell et al., 2006). An atmospheric pressure photoionization (APPI) source (Thermo Fisher Scientific, San Jose, CA) was coupled to the first stage of a custom-built FT-ICR mass spectrometer (see below) through a custom-built interface (Purcell et al., 2006). The tube lens was set to 50 V (to minimize ion fragmentation) and heated metal capillary current was 4.5 A. A Hamilton gastight syringe (5.0 mL) and syringe pump were used to deliver the sample (50 μL/min) to the heated vaporizer region (350°C) of the APPI source, where $N_2$ sheath gas (50 psi) facilitates nebulization. The auxiliary port remained plugged. After nebulization, gas-phase neutral analyte molecules exit the heated vaporizer region as a confined jet. A krypton vacuum UV gas discharge lamp (Syagen Technology, Inc., Tustin, CA) produces 10–10.2 eV photons (120 nm). Toluene increases the ionization efficiency for nonpolar aromatic compounds through dopant-assisted APPI (Robb and Blades, 2006; Robb et al., 2000) through charge exchange, (Purcell et al., 2007b; Smith et al., 2009) and proton transfer (Purcell et al., 2007a) reactions between ionized toluene molecules and neutral analyte molecules as previously reported.

All samples were analyzed with a custom-built FT-ICR mass spectrometer (Kaiser et al., 2011a) equipped with a 22 cm horizontal room temperature bore 9.4 T superconducting solenoid magnet (Oxford Instruments, Abingdon, UK), and a modular ICR data station (Predator) (Blakney et al., 2011) facilitated instrument control, data acquisition, and data analysis. Positive ions generated at atmospheric pressure enter the skimmer region (~2 Torr) through a heated metal capillary, pass through the first radiofrequency (rf)-only octopole, pass through an rf-only quadrupole, and are externally accumulated (Senko et al., 1997) (25–50 ms) in a second octopole equipped with tilted wire extraction electrodes for improved ion extraction and transmission (Wilcox et al., 2002). Helium gas introduced during accumulation collisionally cools ions prior to transfer through rf-only quadrupoles (total length 127 cm) (into a 7-segment open cylindrical cell with capacitively coupled excitation electrodes based on the Tolmachev configuration (Tolmachev et al., 2008; Kaiser et al., 2011b). 100 individual transients of 6.8 s duration were signal averaged. The data was collected at the maximum memory depth of the data station hardware (16 million samples), apodized with a single sided Hanning apodization, zero-filled to 16 megasample (16777216 samples or 224). An additional zero fill brings the preFT data packet to 32 megasample, which in turn is processed via absorption-mode FT analysis (Xian et al., 2010, 2012). Experimentally measured masses were converted from the International Union of Pure and Applied Chemistry (IUPAC) mass scale to the Kendrick mass scale (Kendrick, 1963) for rapid identification of homologous series for each heteroatom class (i.e., species with the same $C_cH_hN_nO_oS_s$ content, differing only be degree of alkylation) (Hughey et al., 2001).

For each elemental composition, $C_cH_hN_nO_oS_s$, the heteroatom class, type (double bond equivalents, DBE = number of rings plus double bonds to carbon, DBE = C − h/2 + n/2 + 1), (Mclafferty and Turecek, 1993) and carbon number, c, were tabulated for subsequent generation of heteroatom class relative abundance distributions and graphical relative-abundance weighted DBE versus carbon number images. Peaks with signal magnitude greater than 6 times the baseline root-mean-square noise at *m/z* 500 were exported to peak lists, internally calibrated based on the "walking calibration" (Savory et al., 2011) and molecular

formula assignments and data visualization were performed with PetroOrg software (Corilo, 2014) Molecular formula assignments with an error >0.5 ppm were discarded, and only chemical classes with a combined relative abundance of $\geq$0.15% of the total were considered. For all mass spectra, the achieved spectral resolving power approached the theoretical limit over the entire mass range: for example, average resolving power, $m/\Delta_{m50\%,}$ in which $\Delta m_{50\%}$ is mass spectral peak full width at half-maximum peak height, was ~1 000 000–1 500 000 at *m/z* 500.